Rapid Communications

Manipulating magnetism in the topological semimetal $EuCd_2As_2$

Na Hyun Jo,[1,2,*] Brinda Kuthanazhi,[1,2,*] Yun Wu,[1,2] Erik Timmons,[1,2] Tae-Hoon Kim,[1] Lin Zhou,[1] Lin-Lin Wang,[1] Benjamin G. Ueland,[1,2] Andriy Palasyuk,[1] Dominic H. Ryan,[3] Robert J. McQueeney,[1,2] Kyungchan Lee,[1,2] Benjamin Schrunk,[1,2] Anton A. Burkov,[4] Ruslan Prozorov,[1,2] Sergey L. Bud'ko,[1,2] Adam Kaminski,[1,2] and Paul C. Canfield[1,2,†]

[1]*Ames Laboratory, Iowa State University, Ames, Iowa 50011, USA*
[2]*Department of Physics and Astronomy, Iowa State University, Ames, Iowa 50011, USA*
[3]*Physics Department and Centre for the Physics of Materials, McGill University, Montreal, Québec, Canada H3A 2T8*
[4]*Department of Physics and Astronomy, University of Waterloo, Waterloo, Ontario, Canada N2L 3G1*

(Received 31 January 2020; revised manuscript received 9 March 2020; accepted 12 March 2020; published 7 April 2020)

$EuCd_2As_2$ is a magnetic semimetal that has the potential of manifesting nontrivial electronic states, depending on its low temperature magnetic ordering. Here, we report the successful synthesis of single crystals of $EuCd_2As_2$ that order ferromagnetically or antiferromagnetically depending on the level of band filling, thus allowing for the use of magnetism to tune the topological properties within the same host. We explored their physical properties via magnetization, electrical transport, heat capacity, and angle-resolved photoemission spectroscopy measurements and conclude that $EuCd_2As_2$ is an excellent, tunable system for exploring the interplay of magnetic ordering and topology.

DOI: 10.1103/PhysRevB.101.140402

Magnetic Weyl semimetals are expected to have extraordinary physical properties such as a chiral anomaly and large anomalous Hall effects that may be useful for future, potential, spintronics applications [1,2]. To date, a number of magnetic topological materials have been proposed. GdPtBi [3] is a proposed magnetic field driven Weyl semimetal [4]. Multiple Weyl points were found in the canted antiferromagnetic state of $YbMnBi_2$ [5]. Furthermore, interesting topological features have been observed in some ferromagnetic kagome lattice materials including $Co_3Sn_2S_2$ [6], Fe_3Sn_2 [7], and FeSn [8]. To be more specific, theoretical predictions suggested three pairs of Weyl points in $Co_3Sn_2S_2$ with out-of-plane ferromagnetic order, and a giant anomalous Hall effect and angle-resolved photoemission spectroscopy (ARPES) results support this scenario [6,9–11]. Fe_3Sn_2 has two Dirac cones with a 30-meV gap near the Fermi level [7]. A flat band and a pair of Dirac bands were observed in FeSn [8]. However, a material with a single pair of Weyl points that readily offers tuning of its topological states is yet to be found.

Recently, the layered triangular lattice compound $EuCd_2As_2$ was identified as a possible antiferromagnetic (AFM) Dirac semimetal with a single Dirac cone located close to the Fermi level when its in-plane, threefold symmetry is preserved [12]. Subsequently, density functional theory (DFT) calculations on $EuCd_2As_2$ predicted that a ferromagnetic (FM) ordered state with Eu moments aligned out of plane can split the Dirac cone into a single pair of Weyl points [13]. However, previous experimental studies on $EuCd_2As_2$ show an A-type AFM below $T_N \simeq 9.5$ K that consists of FM triangular layers stacked antiferromagnetically, with moments pointing in the layer [14–16]. Unfortunately, the in-plane threefold symmetry is broken in this spin configuration. In this case, the Dirac cone is no longer protected and a gap opens [16]. Very recently, an ARPES study above the AFM transition temperature claimed that the effective breaking of time-reversal symmetry by FM-like fluctuations, associated with strong intralayer FM correlations of the A-type AFM order, can induce Weyl nodes [17]. In addition, Soh *et al.* [18] reported a single pair of Weyl nodes in the spin polarized state of $EuCd_2As_2$. All of these results point toward the importance of stabilizing a FM state in $EuCd_2As_2$.

Here, by discovering and taking advantage of the chemical tunability of $EuCd_2As_2$, we report the successful growths of single crystals of $EuCd_2As_2$ with two different magnetic ground states: $EuCd_2As_2$ that orders magnetically at low temperatures with a ferromagnetic component to its long-range order (FM-$EuCd_2As_2$) and $EuCd_2As_2$ that orders magnetically at low temperatures without any detectable ferromagnetic component (AFM-$EuCd_2As_2$). Whereas for many local moment compounds, the desire to tune or change an AFM state to a FM state can be considered to be an unachievable pipe dream, in some cases, chemical substitutions, or even just widths of formation, can be used to accomplish just this feat. For example in the simple, binary, $CeGe_{2-x}$ system, depending on the value of x, there can be either a FM or AFM transition [19]. Based on our DFT calculations [13], we expect to have a topological insulator in the AFM-$EuCd_2As_2$ and two pairs of Weyl points in the FM-$EuCd_2As_2$. In addition, a single pair of Weyl points can be further realized with a magnetic field applied along the crystallographic c direction (see Supplemental Material [20]).

*These authors contributed equally to this work.
†canfield@ameslab.gov

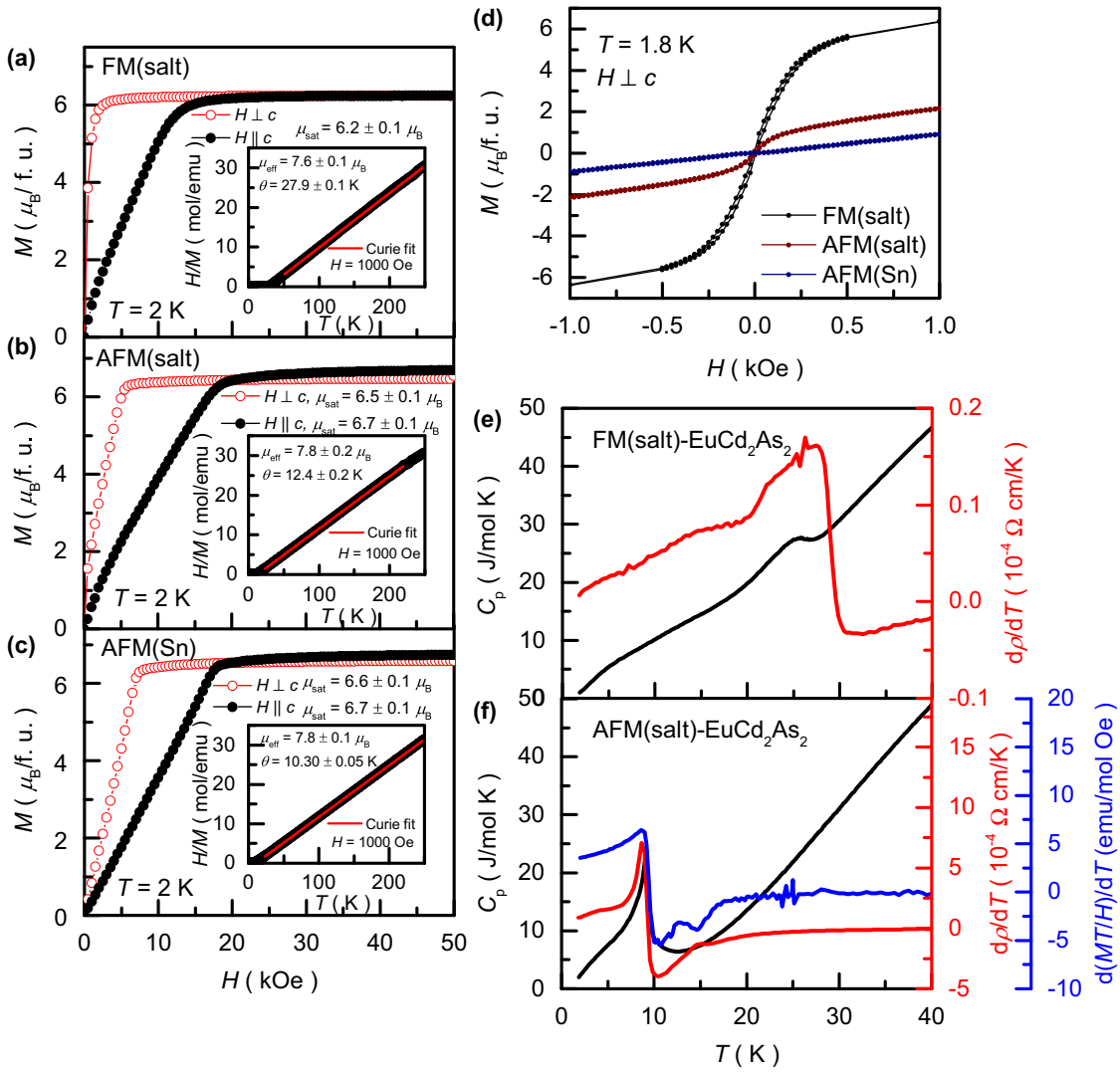

FIG. 1. Specific heat, resistivity, and magnetization data for FM-$EuCd_2As_2$ and AFM-$EuCd_2As_2$. (a)–(c) Magnetic field dependent magnetization with the field parallel to the c axis (black filled circle) and perpendicular to the c axis (red open circle) at 2 K for FM-$EuCd_2As_2$, AFM-$EuCd_2As_2$, and Sn flux grown AFM-$EuCd_2As_2$, respectively. Inset shows the inverse susceptibility with Curie-Weiss fitting. (d) A comparison between the magnetic field dependent magnetization for the three samples, FM-$EuCd_2As_2$, AFM-$EuCd_2As_2$, and Sn flux grown AFM-$EuCd_2As_2$, in the low-field regime between -1000 Oe and 1000 Oe. All the measurements shown were done with the field perpendicular to the c axis. (e) Temperature dependent specific heat C_P (black line, left axis) and resistivity derivatives (red line, right axis) for FM-$EuCd_2As_2$. (f) Temperature dependent specific heat C_P (black line, left axis), resistivity derivatives (red line, right axis), and $d(MT/H)/dT$ at $H_{\|c} = 50$ Oe (blue line, the second right axis) for AFM-$EuCd_2As_2$.

Single crystals of both FM-$EuCd_2As_2$ and AFM-$EuCd_2As_2$ were grown via solution growth using a salt mixture as flux. The difference in growth procedure between FM-$EuCd_2As_2$ and AFM-$EuCd_2As_2$ was the initial stoichiometry of Eu:Cd:As in the salt mixture. We also grew single crystals of $EuCd_2As_2$ using Sn flux and these crystals also manifest AFM order. We confirmed the crystal structure and composition via x-ray diffraction patterns and scanning transmission electron microscopy (STEM) with energy dispersive spectroscopy (EDS) (see Supplemental Material for more details of crystal growth and experiments [20]).

In order to determine the transition temperatures and nature of the magnetic ground state in these crystals, we conducted specific heat, resistivity, and magnetization measurements. Figures 1(a)–1(c) show the anisotropic $M(H)$ and $H/M(T)$ data for the three representative crystals we have studied: FM(salt)-$EuCd_2As_2$, AFM(salt)-$EuCd_2As_2$, and AFM(Sn)-$EuCd_2As_2$. At $T = 2$ K, each of these samples becomes saturated by roughly 20 kOe for $H \| c$; for $H \perp c$, the $M(H)$ data saturates at progressively lower and lower fields as we progress from AFM(Sn) to AFM(salt) to FM(salt). All samples display a magnetic easy axis that lies within the layers. Whereas the $H \perp c$ data in Fig. 1(a) suggests a FM state, Fig. 1(d) shows that, indeed, the FM(salt) sample develops an unambiguous remanent magnetization at $H = 0$ for full, four-quadrant $M(H)$ loops. Other differences between these samples include FM(salt) having a resolvably lower $\mu_{\rm sat}$ and $\mu_{\rm eff}$ and higher Curie-Weiss theta value than the AFM

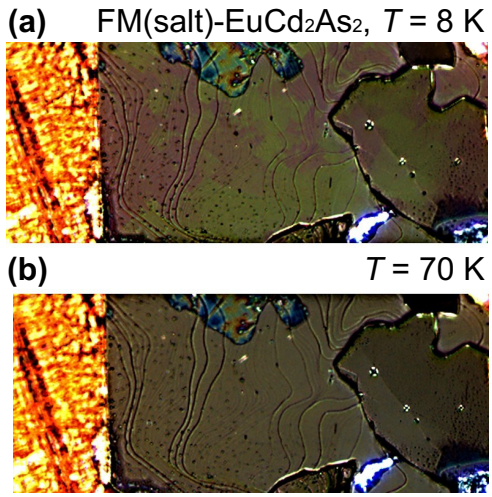

FIG. 2. Magneto-optical image of FM(salt)-$EuCd_2As_2$. (a) Imaged at $T = 8$ K, ferromagnetic domains (brown and green colors) appear below T_C. (b) Absence of domains above the magnetic transition, here imaged at $T = 70$ K. Copper-color area on the left in each image is the copper sample holder.

samples. These data suggest that FM(salt) samples have less than the full Eu^{2+} occupancy of the Eu sites. This is consistent with multiple powder x-ray data sets we have collected and analyzed. Both laboratory-based as well as synchrotron-based data indicate that the FM(salt) sample has Eu vacancies at the several percent level. (see Supplemental Material at [20]). At a finer level of comparison, the AFM(salt) sample is closer to the AFM(Sn) sample, but intermediate in its $M(H)$ behavior at 1.8 K and Curie-Weiss temperature value. This is an observation that we will return to once we present our ARPES data in Fig. 3 below.

We can also compare the behavior of FM(salt) and AFM(salt) near their respective transition temperatures. FM(salt) has a broader, and much higher temperature, feature than AFM(salt) in the specific heat data as shown in Figs. 1(e) and 1(f), respectively. Using the peak position as a criterion, the transition temperature for FM(salt) is $T_C \simeq 26.4$ K, and the transition temperature for AFM(salt) is $T_N \simeq 9.2$ K. Note that AFM(Sn) has a similar transition temperature as that found for AFM(salt). The peak position of the magnetic susceptibility data when the applied magnetic field was parallel to c is the same for AFM(salt) and AFM(Sn) (see Supplemental Material [20]). In addition to these transitions, both $EuCd_2As_2$ samples have a broad shoulder at temperatures below T_N of T_C. The origin of this additional anomaly can be attributed to the thermal population of the $4f$ crystal-field levels that are split by the molecular field acting on Eu ions [47].

Figures 1(e) and 1(f) also show temperature dependent resistivity derivatives ($d\rho/dT$) of FM(salt) and AFM(salt) samples (see Supplemental Material for $\rho(T)$ data [20]). Near the magnetic transition temperature, $d\rho/dT$ is found to resemble the specific heat [48]. Clear signatures of a phase transition are observed for both FM(salt) and AFM(salt).

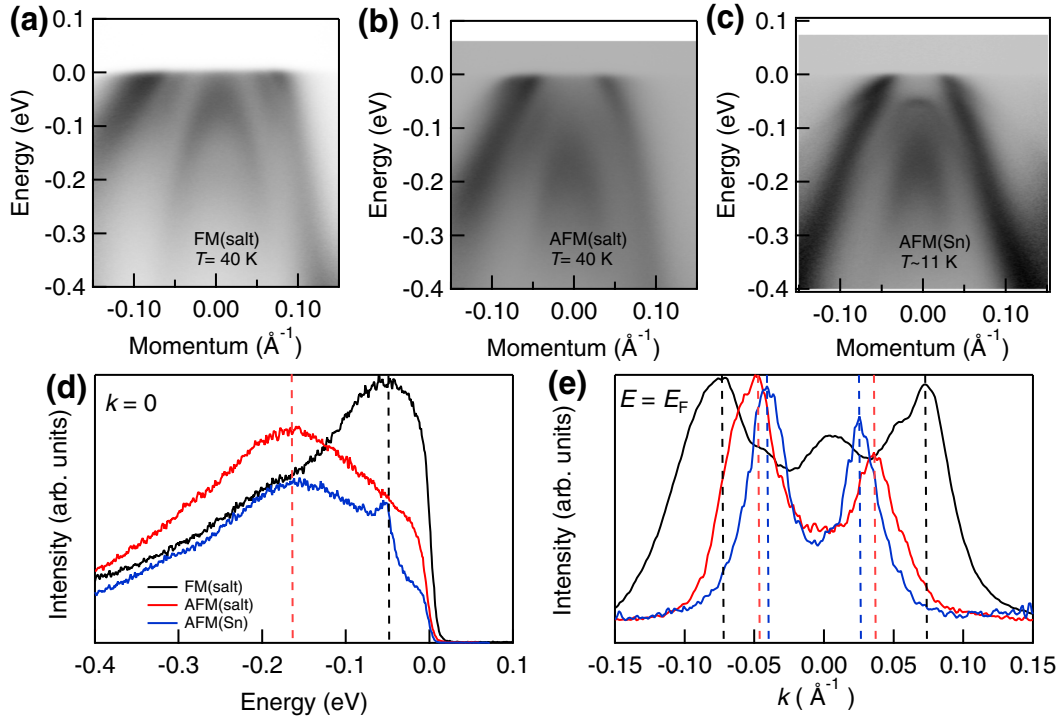

FIG. 3. ARPES measurement of the band structure of FM(salt)-$EuCd_2As_2$, AFM(salt)-$EuCd_2As_2$, and AFM(Sn)-$EuCd_2As_2$. ARPES intensity plot along a cut through the gamma point for (a) FM(salt) at $T = 40$ K. (b) AFM(salt) at $T = 40$ K. (c) Electronic structure of AFM(Sn) at $T \sim 11$ K. (d) Energy distribution curve at the zero momentum of FM(salt), AFM(salt), and AFM(Sn) with black, red, and blue lines, respectively. Dashed lines indicate the energy of the top of the inner hole band for FM(salt) and AFM(salt). (e) Momentum distribution curves (MDCs) at E_F of FM(salt), AFM(salt), and AFM(Sn) with black, red, and blue lines, respectively. Dashed lines [black for FM(salt), red for AFM(salt), and blue for AFM(Sn)] are indicating the peak positions of MDCs that mark the value of the Fermi momentum.

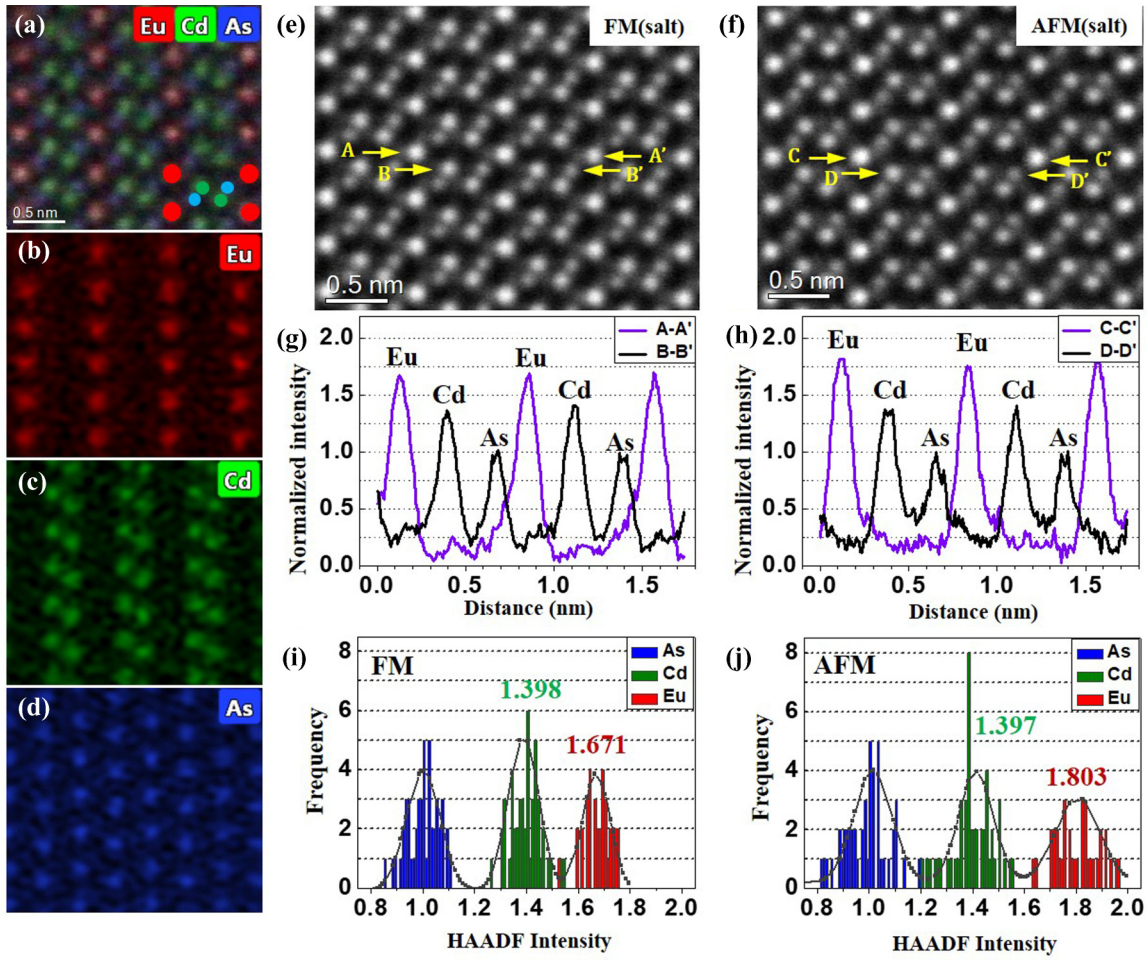

FIG. 4. HAADF-STEM and EDS analysis of FM(salt)-$EuCd_2As_2$ and AFM(salt)-$EuCd_2As_2$ along [21 $\bar{1}$ $\bar{0}$] zone axis. (a) High-resolution HAADF-STEM image of FM(salt) superimposed with color composite EDS elemental maps, and overlaid atomic model. (b)–(d) Atomically resolved EDS map of Eu, Cd, and As taken from the same area of (a). (e),(f) High-resolution HAADF image of FM(salt) and AFM(salt), respectively. (g),(h) Line profiles showing the image intensity (normalized to equal one for the As column) as a function of position in image (e) along A-A′ and B-B′, and positions in image (f) along C-C′ and D-D′, respectively. (i),(j) Histogram of the intensities of atomic image maxima in the area of (e) and (f), respectively.

Figure 1(f) also shows the temperature dependent $\frac{d(MT/H)}{dT}$ at $H = 50$ Oe along the crystallographic c axis on AFM(salt) which also reveals a feature similar to that seen in the specific heat data [49]; this analysis is formally only appropriate for AFM transitions (not FM ones) and is not shown in Fig. 1(e).

To confirm the FM nature of FM(salt) samples, magneto-optical images were taken at temperatures above and below the transition temperature (see Fig. 2 as well as the Supplemental Material [20]), and comparison reveals the formation of magnetic domains below the transition. Similar imaging was performed on AFM(salt) but no domains were detected at any temperature (see Supplemental Material for more details of crystal growth and experiments [20]). In addition to the observation of hysteresis, the ferromagnetic domains seen in Fig. 2 (and studied in further detail in the Supplemental Material [20]) provide a second, clear, indication that there is a net ferromagnetic component to the ordered state in FM(salt) [50]. On the other hand, the data shown in Fig. 1(d) and Supplemental Material Fig. S7 are consistent with an antiferromagnetic ground state of AFM(salt) [20].

In order to probe the possible electronic origins that distinguish the FM(salt), AFM(salt), and AFM(Sn) samples, ARPES measurements were performed at low temperature (see Fig. 3). The data clearly show changes in the band filling: there is an almost rigid band shift of the hole pocket that crosses E_F to higher binding energy as we progress from FM(salt) to AFM(salt) to AFM(Sn). Energy distribution curves at the Γ point shown in Fig. 3(d) also demonstrate that the top of the inner hole band of FM(salt) is ∼120 meV higher than that of AFMs. In addition, we observe a smaller size of the pocket in momentum distribution curve at the E_F [see Fig. 3(e)] The difference in the band filling between FM(salt), AFM(salt), and AFM(Sn) could be associated with either Eu-site occupancy or the ratio of divalent to trivalent (nonmagnetic) Eu.

To better correlate the differences in magnetization and band filling between FM(salt) and AFM(salt) with possible composition differences, we performed STEM on both FM(salt) and AFM(salt). The results suggest more Eu vacancies in FM(salt). Color composite, high-resolution high-angle-annular-dark-field (HAADF) scanning transmission electron

microscopy (STEM) image, and EDS elemental mapping of FM(salt) along the [21 $\bar{1}$ $\bar{0}$] crystallographic direction [Figs. 4(a)–4(d)] clearly demonstrate individual Eu, Cd, and As atomic columns. To reveal any possible Eu and Cd site occupancy difference in AFM(salt) and FM(salt) samples, we directly compared the intensity of Eu, Cd and As columns in HAADF images of both samples [Figs. 4(e) and 4(f)] [51]. The images were taken under the same experimental conditions and sample thickness (∼10 nm). Figures 4(g) and 4(h) show line profiles through the two locations marked in Figs. 4(e) and 4(h), respectively. The intensities were normalized to equal one for the As column. Profiles A-A′ and C-C′ indicate the intensity of Eu columns, and profiles B-B′ and D-D′ show the intensity of Cd-As pairs. The Eu column of FM(salt) shows slightly lower intensity (∼1.7) than that of AFM(salt) (∼1.8), whereas the Cd column indicates almost the same intensity. Figures 4(i) and 4(j) show a histogram of the normalized peak intensities (As peak as 1) for all the atoms in Figs. 4(e) and 4(f), respectively. A theoretical Gaussian fit [51] for the distributions of the different species of the atoms, based on the standard deviations determined experimentally for the Eu, Cd, and As atoms is overlaid on the figure. It is clearly demonstrated that the Eu column of FM(salt) has lower average intensity (1.671) than that of AFM(salt) (1.803), suggesting more vacancies in FM(salt). The TEM results are also consistent with the x-ray results shown in the Supplemental Material [20]. In addition, the presence of Eu vacancies in FM samples, which will lower the electron count, is also consistent with ARPES data indicating a lower E_F.

Our results show that $EuCd_2As_2$ is a rare material that can be tuned from having an antiferromagnetic ground state to a ferromagnetic one. By changing growth conditions, $EuCd_2As_2$ can be shifted from a $T_N \simeq 9.2$ K antiferromagnet to a $T_C \simeq 26.4$ K ferromagnet. This change in ground state is associated with a clear shift in the electronic structure as well as measured Eu^{2+} content. Detailed DFT calculations predict that the AFM state is a host to topological insulators, while the FM state hosts two pairs of Weyl points. This can be further tuned to one pair of Weyl points by polarizing spins along the crystallographic c direction. This material is therefore an ideal candidate for studies of the interplay of magnetism and topology and the macroscopic manifestation of Weyl fermions.

Relevant data for the work are available at the Materials Data Facility Ref. [52].

The authors thank A. Bhattacharya and R. McDonald for helpful discussion. This work was supported by the U.S. Department of Energy, Office of Basic Energy Sciences, Division of Materials Sciences and Engineering. The research (N.H.J., Y.W., E.T., A.P., D.H.R., K.L., B.S., R.P., S.L.B., and P.C.C.) was performed at Ames Laboratory. Ames Laboratory is operated for the U.S. Department of Energy by the Iowa State University under Contract No. DE-AC02-07CH11358. This work was also supported by the Center for Advancement of Topological Semimetals (N.H.J., B.K., L.-L.W, B.G.U., R.J.M., A.A.B., and A.K.), an Energy Frontier Research Center funded by the U.S. Department of Energy Office of Science, Office of Basic Energy Sciences, through the Ames Laboratory under its Contract No. DE-AC02-07CH11358. Use of the Advanced Photon Source at Argonne National Laboratory was supported by the U.S. Department of Energy (DOE), Office of Science, Office of Basic Energy Sciences, under Contract No. DE-AC02-06CH11357. T.-H.K. and L.Z. are supported by Laboratory Directed Research and Development funds through Ames Laboratory. All TEM and related work were performed using instruments in the Sensitive Instrument Facility in Ames Laboratory. D.H.R. is also supported by Fonds Québécois de la Recherche sur la Nature et les Technologies.

[1] B. Yan and C. Felser, Ann. Rev. Condens. Matter Phys. **8**, 337 (2017).
[2] Steven S.-L. Zhang, A. A. Burkov, I. Martin, and O. G. Heinonen, Phys. Rev. Lett. **123**, 187201 (2019).
[3] P. C. Canfield, J. Thompson, W. Beyermann, A. Lacerda, M. Hundley, E. Peterson, Z. Fisk, and H. Ott, J. Appl. Phys. **70**, 5800 (1991).
[4] M. Hirschberger, S. Kushwaha, Z. Wang, Q. Gibson, S. Liang, C. A. Belvin, B. A. Bernevig, R. J. Cava, and N. P. Ong, Nat. Mater. **15**, 1161 (2016).
[5] S. Borisenko, D. Evtushinsky, Q. Gibson, A. Yaresko, K. Koepernik, T. Kim, M. Ali, J. van den Brink, M. Hoesch, A. Fedorov, E. Haubold, Y. Kushnirenko, I. Soldatov, R. Schäfer, and R. J. Cava, Nat. Commun. **10**, 3424 (2019).
[6] E. Liu, Y. Sun, N. Kumar, L. Muechler, A. Sun, L. Jiao, S.-Y. Yang, D. Liu, A. Liang, Q. Xu *et al.*, Nat. Phys. **14**, 1125 (2018).
[7] L. Ye, M. Kang, J. Liu, F. Von Cube, C. R. Wicker, T. Suzuki, C. Jozwiak, A. Bostwick, E. Rotenberg, D. C. Bell *et al.*, Nature (London) **555**, 638 (2018).
[8] M. Kang, L. Ye, S. Fang, J.-S. You, A. Levitan, M. Han, J. I. Facio, C. Jozwiak, A. Bostwick, E. Rotenberg *et al.*, Nat. Mater. **19**, 163 (2020).
[9] X. Lin, S. L. Bud'ko, and P. C. Canfield, Philos. Mag. **92**, 2436 (2012).
[10] Q. Xu, E. Liu, W. Shi, L. Muechler, J. Gayles, C. Felser, and Y. Sun, Phys. Rev. B **97**, 235416 (2018).
[11] D. Liu, A. Liang, E. Liu, Q. Xu, Y. Li, C. Chen, D. Pei, W. Shi, S. Mo, P. Dudin, T. Kim, C. Cacho, G. Li, Y. Sun, L. X. Yang, Z. K. Liu, S. S. P. Parkin, C. Felser, and Y. L. Chen, Science **365**, 1282 (2019).
[12] G. Hua, S. Nie, Z. Song, R. Yu, G. Xu, and K. Yao, Phys. Rev. B **98**, 201116(R) (2018).
[13] L.-L. Wang, N. H. Jo, B. Kuthanazhi, Y. Wu, R. J. McQueeney, A. Kaminski, and P. C. Canfield, Phys. Rev. B **99**, 245147 (2019).
[14] I. Schellenberg, U. Pfannenschmidt, M. Eul, C. Schwickert, and R. Pöttgen, Z. Anorg. Allg. Chem. **637**, 1863 (2011).
[15] H. P. Wang, D. S. Wu, Y. G. Shi, and N. L. Wang, Phys. Rev. B **94**, 045112 (2016).

[16] M. C. Rahn, J.-R. Soh, S. Francoual, L. S. I. Veiga, J. Strempfer, J. Mardegan, D. Y. Yan, Y. F. Guo, Y. G. Shi, and A. T. Boothroyd, Phys. Rev. B **97**, 214422 (2018).

[17] J.-Z. Ma, S. Nie, C. Yi, J. Jandke, T. Shang, M. Yao, M. Naamneh, L. Yan, Y. Sun, A. Chikina *et al.*, Sci. Adv. **5**, eaaw4718 (2019).

[18] J.-R. Soh, F. de Juan, M. G. Vergniory, N. B. M. Schröter, M. C. Rahn, D. Y. Yan, J. Jiang, M. Bristow, P. Reiss, J. N. Blandy, Y. F. Guo, Y. G. Shi, T. K. Kim, A. McCollam, S. H. Simon, Y. Chen, A. I. Coldea, and A. T. Boothroyd, Phys. Rev. B **100**, 201102(R) (2019).

[19] S. L. Bud'ko, H. Hodovanets, A. Panchula, R. Prozorov, and P. C. Canfield, J. Phys.: Condens. Matter **26**, 146005 (2014).

[20] See Supplemental Material at http://link.aps.org/supplemental/10.1103/PhysRevB.101.140402 for detailed experimental methods, DFT calculation, and additional or elaborations on experimental (x-ray diffractions, electron diffraction patterns, temperature dependent resistivity, magneto optics, and anisotropic magnetization data) results. The Supplemental Material includes Refs. [14,16,17,21–46].

[21] P. C. Canfield, T. Kong, U. S. Kaluarachchi, and N. H. Jo, Philos. Mag. **96**, 84 (2016).

[22] A. Kreyssig, R. Prozorov, C. D. Dewhurst, P. C. Canfield, R. W. McCallum, and A. I. Goldman, Phys. Rev. Lett. **102**, 047204 (2009).

[23] M. A. Tanatar, A. Kreyssig, S. Nandi, N. Ni, S. L. Bud'ko, P. C. Canfield, A. I. Goldman, and R. Prozorov, Phys. Rev. B **79**, 180508(R) (2009).

[24] R. Jiang, D. Mou, Y. Wu, L. Huang, C. D. McMillen, J. Kolis, H. G. Giesber, J. J. Egan, and A. Kaminski, Rev. Sci. Instrum. **85**, 033902 (2014).

[25] P. Hohenberg and W. Kohn, Phys. Rev. **136**, B864 (1964).

[26] W. Kohn and L. J. Sham, Phys. Rev. **140**, A1133 (1965).

[27] P. E. Blöchl, Phys. Rev. B **50**, 17953 (1994).

[28] G. Kresse and J. Furthmüller, Phys. Rev. B **54**, 11169 (1996).

[29] G. Kresse and J. Furthmüller, Comput. Mater. Sci **6**, 15 (1996).

[30] S. L. Dudarev, G. A. Botton, S. Y. Savrasov, C. J. Humphreys, and A. P. Sutton, Phys. Rev. B **57**, 1505 (1998).

[31] H. J. Monkhorst and J. D. Pack, Phys. Rev. B **13**, 5188 (1976).

[32] N. Marzari and D. Vanderbilt, Phys. Rev. B **56**, 12847 (1997).

[33] I. Souza, N. Marzari, and D. Vanderbilt, Phys. Rev. B **65**, 035109 (2001).

[34] N. Marzari, A. A. Mostofi, J. R. Yates, I. Souza, and D. Vanderbilt, Rev. Mod. Phys. **84**, 1419 (2012).

[35] D. H. Lee and J. D. Joannopoulos, Phys. Rev. B **23**, 4988 (1981).

[36] D. H. Lee and J. D. Joannopoulos, Phys. Rev. B **23**, 4997 (1981).

[37] M. P. L. Sancho, J. M. L. Sancho, and J. Rubio, J. Phys. F **14**, 1205 (1984).

[38] M. P. L. Sancho, J. M. L. Sancho, J. M. L. Sancho, and J. Rubio, J. Phys. F **15**, 851 (1985).

[39] Q. Wu, S. Zhang, H.-F. Song, M. Troyer, and A. A. Soluyanov, Comput. Phys. Commun. **224**, 405 (2018).

[40] R. S. K. Mong, A. M. Essin, and J. E. Moore, Phys. Rev. B **81**, 245209 (2010).

[41] J. Rodríguez-Carvajal, Phys. B (Amsterdam, Neth.) **192**, 55 (1993).

[42] J. Wang, B. H. Toby, P. L. Lee, L. Ribaud, S. M. Antao, C. Kurtz, M. Ramanathan, R. B. Von Dreele, and M. A. Beno, Rev. Sci. Instrum. **79**, 085105 (2008).

[43] P. L. Lee, D. Shu, M. Ramanathan, C. Preissner, J. Wang, M. A. Beno, R. B. Von Dreele, L. Ribaud, C. Kurtz, S. M. Antao *et al.*, J. Synchrotron Radiat. **15**, 427 (2008).

[44] B. H. Toby, Y. Huang, D. Dohan, D. Carroll, X. Jiao, L. Ribaud, J. A. Doebbler, M. R. Suchomel, J. Wang, C. Preissner *et al.*, J. Appl. Crystallogr. **42**, 990 (2009).

[45] A. C. Larson and R. B. Von Dreele, Los Alamos National Laboratory Report LAUR 86, 1994.

[46] B. H. Toby, J. Appl. Crystallogr. **34**, 210 (2001).

[47] C. Marquina, N.-T. H. Kim-Ngan, K. H. J. Buschow, J. J. M. Franse, and M. R. Ibarra, J. Magn. Magn. Mater. **157-158**, 403 (1996).

[48] M. E. Fisher and J. S. Langer, Phys. Rev. Lett. **20**, 665 (1968).

[49] M. E. Fisher, Philos. Mag. **7**, 1731 (1962).

[50] S.-W. Cheong, M. Fiebig, W. Wu, L. Chapon, and V. Kiryukhin, npj Quantum Mater. **5**, 1 (2020).

[51] O. L. Krivanek, M. F. Chisholm, V. Nicolosi, T. J. Pennycook, G. J. Corbin, N. Dellby, M. F. Murfitt, C. S. Own, Z. S. Szilagyi, M. P. Oxley *et al.*, Nature (London) **464**, 571 (2010).

[52] https://doi.org/10.18126/m1ci-avjm.